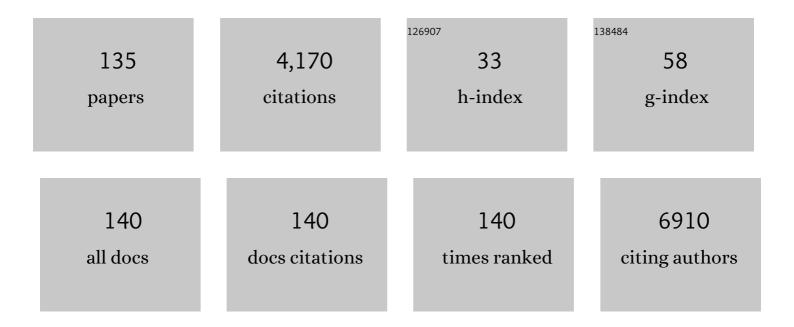
List of Publications by Year in descending order

Source: https://exaly.com/author-pdf/283134/publications.pdf Version: 2024-02-01



#	Article	IF	CITATIONS
1	Exciton dynamics and annihilation in WS <sub>2</sub> 2D semiconductors. Nanoscale, 2015, 7, 7402-7408.	5.6	388
2	Twist-angle-dependent interlayer exciton diffusion in WS2–WSe2 heterobilayers. Nature Materials, 2020, 19, 617-623.	27.5	193
3	Exciton Dynamics, Transport, and Annihilation in Atomically Thin Two-Dimensional Semiconductors. Journal of Physical Chemistry Letters, 2017, 8, 3371-3379.	4.6	169
4	Long-range exciton transport and slow annihilation in two-dimensional hybrid perovskites. Nature Communications, 2020, 11, 664.	12.8	167
5	Photocarrier generation from interlayer charge-transfer transitions in WS <sub>2</sub> -graphene heterostructures. Science Advances, 2018, 4, e1700324.	10.3	160
6	Carbon-protected bimetallic carbide nanoparticles for a highly efficient alkaline hydrogen evolution reaction. Nanoscale, 2015, 7, 3130-3136.	5.6	133
7	Highly mobile charge-transfer excitons in two-dimensional WS <sub>2</sub> /tetracene heterostructures. Science Advances, 2018, 4, eaao3104.	10.3	132
8	Sn–Ni <sub>3</sub> S <sub>2</sub> Ultrathin Nanosheets as Efficient Bifunctional Water-Splitting Catalysts with a Large Current Density and Low Overpotential. ACS Applied Materials & Interfaces, 2018, 10, 40568-40576.	8.0	113
9	Beneficial and Adverse Effects of an LXR Agonist on Human Lipid and Lipoprotein Metabolism and Circulating Neutrophils. Cell Metabolism, 2016, 24, 223-233.	16.2	109
10	Engineering the surface of perovskite La <sub>0.5</sub> Sr <sub>0.5</sub> MnO <sub>3</sub> for catalytic activity of CO oxidation. Chemical Communications, 2014, 50, 9200-9203.	4.1	84
11	Improved Doping and Emission Efficiencies of Mn-Doped CsPbCl <sub>3</sub> Perovskite Nanocrystals via Nickel Chloride. Journal of Physical Chemistry Letters, 2019, 10, 4177-4184.	4.6	79
12	Extrinsic and Dynamic Edge States of Two-Dimensional Lead Halide Perovskites. ACS Nano, 2019, 13, 1635-1644.	14.6	79
13	Crystal facet tailoring arts in perovskite oxides. Inorganic Chemistry Frontiers, 2015, 2, 965-981.	6.0	78
14	Ultrafast Dynamic Microscopy of Carrier and Exciton Transport. Annual Review of Physical Chemistry, 2019, 70, 219-244.	10.8	75
15	Direct Chemical-Vapor-Deposition-Fabricated, Large-Scale Graphene Glass with High Carrier Mobility and Uniformity for Touch Panel Applications. ACS Nano, 2016, 10, 11136-11144.	14.6	69
16	Antioxidant Effects of Lycopene in African American Men with Prostate Cancer or Benign Prostate Hyperplasia: A Randomized, Controlled Trial. Cancer Prevention Research, 2011, 4, 711-718.	1.5	67
17	Activation of Surface Oxygen Sites in a Cobalt-Based Perovskite Model Catalyst for CO Oxidation. Journal of Physical Chemistry Letters, 2018, 9, 4146-4154.	4.6	67
18	δ-MnO <sub>2</sub> –Mn <sub>3</sub> O <sub>4</sub> Nanocomposite for Photochemical Water Oxidation: Active Structure Stabilized in the Interface. ACS Applied Materials & Interfaces, 2016, 8, 27825-27831.	8.0	60

#	Article	IF	CITATIONS
19	Hydrogenated bilayer wurtzite SiC nanofilms: a two-dimensional bipolar magnetic semiconductor material. Physical Chemistry Chemical Physics, 2013, 15, 497-503.	2.8	55
20	Ultrafast Imaging of Carrier Transport across Grain Boundaries in Hybrid Perovskite Thin Films. ACS Energy Letters, 2018, 3, 1402-1408.	17.4	55
21	Diamondization of chemically functionalized graphene and graphene–BN bilayers. Physical Chemistry Chemical Physics, 2012, 14, 8179.	2.8	52
22	From solid-state metal alkoxides to nanostructured oxides: a precursor-directed synthetic route to functional inorganic nanomaterials. Inorganic Chemistry Frontiers, 2015, 2, 198-212.	6.0	48
23	Crystal Shape Tailoring in Perovskite Structure Rare-Earth Ferrites REFeO <sub>3</sub> (RE = La, Pr, Sm,) Tj ETQq1 Design, 2016, 16, 6522-6530.	1 0.7843 3.0	14 rgBT /0 46
24	Molten Salt Flux Synthesis, Crystal Facet Design, Characterization, Electronic Structure, and Catalytic Properties of Perovskite Cobaltite. ACS Applied Materials & Interfaces, 2018, 10, 28219-28231.	8.0	46
25	Systematic evaluation of the root cause of nonâ€linearity in liquid chromatography/tandem mass spectrometry bioanalytical assays and strategy to predict and extend the linear standard curve range. Rapid Communications in Mass Spectrometry, 2012, 26, 1465-1474.	1.5	44
26	Catalytic behavior of electrospinning synthesized La0.75Sr0.25MnO3 nanofibers in the oxidation of CO and CH4. Chemical Engineering Journal, 2014, 244, 27-32.	12.7	42
27	Low temperature hydrothermal synthesis, structure and magnetic properties of RECrO <sub>3</sub> (RE = La, Pr, Nd, Sm). Dalton Transactions, 2015, 44, 17201-17208.	3.3	42
28	Simple and efficient digestion of a monoclonal antibody in serum using pellet digestion: comparison with traditional digestion methods in LC–MS/MS bioanalysis. Bioanalysis, 2012, 4, 2887-2896.	1.5	39
29	Hydrothermal synthesis and magnetic properties of REFe0.5Cr0.5O3 (RE = La, Tb, Ho, Er, Yb, Lu and Y) perovskite. New Journal of Chemistry, 2014, 38, 1168.	2.8	39
30	Continuous Meltâ€Drawing of Highly Aligned Flexible and Stretchable Semiconducting Microfibers for Organic Electronics. Advanced Functional Materials, 2018, 28, 1705584.	14.9	39
31	Nanoscale Architecture of RuO <sub>2</sub> /La <sub>0.9</sub> Fe <sub>0.92</sub> Ru <sub>0.08–<i>x</i></sub> O <sub>3â~î</sub> Composite via Manipulating the Exsolution of Low Ru-Substituted A-Site Deficient Perovskite. ACS Sustainable Chemistry and Engineering, 2018, 6, 11999-12005.	6.7	39
32	Research on photonic crystal fiber based on a surface plasmon resonance sensor with segmented silver-titanium dioxide film. Journal of the Optical Society of America B: Optical Physics, 2020, 37, 736.	2.1	39
33	"Center punch―and "whole spot―bioanalysis of apixaban in human dried blood spot samples by UHPLC-MS/MS. Journal of Chromatography B: Analytical Technologies in the Biomedical and Life Sciences, 2015, 988, 66-74.	2.3	38
34	Solar selective absorbers with foamed nanostructure prepared by hydrothermal method on stainless steel. Solar Energy Materials and Solar Cells, 2016, 146, 99-106.	6.2	36
35	Growth orientation, shape evolution of monodisperse PbSe nanocrystals and their use in optoelectronic devices. CrystEngComm, 2013, 15, 597-603.	2.6	34
36	Systematic investigation of orthogonal SPE sample preparation for the LC–MS/MS bioanalysis of a monoclonal antibody after pellet digestion. Bioanalysis, 2013, 5, 2379-2391.	1.5	32

LONG YUAN

#	Article	IF	CITATIONS
37	Structure, optical spectroscopy properties and thermochromism of Sm <sub>3</sub> Fe <sub>5</sub> O <sub>12</sub> garnets. Journal of Materials Chemistry C, 2016, 4, 10529-10537.	5.5	32
38	Cation Segregation of A-Site Deficiency Perovskite La <sub>0.85</sub> FeO <sub>3â^î^</sub> Nanoparticles toward High-Performance Cathode Catalysts for Rechargeable Li-O <sub>2</sub> Battery. ACS Applied Materials & Interfaces, 2018, 10, 25465-25472.	8.0	31
39	D-Shaped Photonic Crystal Fiber Plasmonic Sensor Based on Silver-Titanium Dioxide Composite Micro-grating. Plasmonics, 2021, 16, 2049-2059.	3.4	30
40	Estrogen Receptor α Enhances the Rate of Oxidative DNA Damage by Targeting an Equine Estrogen Catechol Metabolite to the Nucleus. Journal of Biological Chemistry, 2009, 284, 8633-8642.	3.4	29
41	Composition dependent magnetic and ferroelectric properties of hydrothermally synthesized GdFe <sub>1â^'x</sub> Cr <sub>x</sub> O <sub>3</sub> (0.1 ≤ ≤0.9) perovskites. Dalton Transactions, 2017, 46, 5930-5937.	3.3	27
42	High ionic conductivity Y doped Li1.3Al0.3Ti1.7(PO4)3 solid electrolyte. Journal of Alloys and Compounds, 2019, 782, 384-391.	5.5	27
43	Hydrothermal synthesis and photoluminescence properties of rare-earth niobate and tantalate nanophosphors. Dalton Transactions, 2013, 42, 8041.	3.3	26
44	Solventâ€Free Synthesis and <i>n</i> â€Hexadecane Hydroisomerization Performance of SAPOâ€11 Catalyst. European Journal of Inorganic Chemistry, 2018, 2018, 2599-2606.	2.0	26
45	Jahn–Teller Disproportionation Induced Exfoliation of Unitâ€Cell Scale ϵâ€MnO <sub>2</sub> . Angewandte Chemie - International Edition, 2020, 59, 22659-22666.	13.8	26
46	Crystal facet control of LaFeO3, LaCrO3, and La0.75Sr0.25MnO3. CrystEngComm, 2014, 16, 2874.	2.6	25
47	Hydrothermal syntheses and photoluminescence properties of rare-earth tungstate as near ultraviolet type red phosphors. New Journal of Chemistry, 2014, 38, 1441.	2.8	25
48	In-situ optical and structural insight of reversible thermochromic materials of Sm3-xBixFe5O12 (x= 0,) Tj ETQq0 (	) 0 <sub>3</sub> rgBT /(	Overlock 10 T
49	Water-assisted synthesis of shape-specific BiOCl nanoflowers with enhanced adsorption and photosensitized degradation of rhodamine B. Environmental Chemistry Letters, 2020, 18, 243-249.	16.2	23
50	Realization of interstitial boron ordering and optimal near-surface electronic structure in Pd-B alloy electrocatalysts. Chemical Engineering Journal, 2021, 419, 129568.	12.7	23
51	Electrochromic response of pulsed laser deposition prepared WO <sub>3</sub> –TiO <sub>2</sub> composite film. RSC Advances, 2014, 4, 47670-47676.	3.6	22
52	Application of a stabilizer cocktail of N-ethylmaleimide and phenylmethanesulfonyl fluoride to concurrently stabilize the disulfide and ester containing compounds in a plasma LC–MS/MS assay. Journal of Pharmaceutical and Biomedical Analysis, 2014, 88, 552-561.	2.8	22
53	Hydrothermal preparation of perovskite structures DyCrO <sub>3</sub> and HoCrO <sub>3</sub> . Dalton Transactions, 2016, 45, 17593-17597.	3.3	22

<sup>&</sup>lt;sup>54</sup> Ultra-low reflection CuO nanowire array in-situ grown on copper sheet. Materials and Design, 2017, 7.0 21 113, 297-304.

#	Article	IF	CITATIONS
55	Low-temperature hydrothermal fabrication of Fe3O4 nanostructured solar selective absorption films. Applied Surface Science, 2018, 458, 629-637.	6.1	21
56	A User-Friendly Robotic Sample Preparation Program for Fully Automated Biological Sample Pipetting and Dilution to Benefit the Regulated Bioanalysis. Journal of the Association for Laboratory Automation, 2012, 17, 211-221.	2.8	20
57	Insight into the enhanced photoelectrocatalytic activity in reduced LaFeO <sub>3</sub> films. Chemical Communications, 2017, 53, 2499-2502.	4.1	20
			ľ

 $\frac{1000}{58}$  Mild Hydrothermal Crystallization of Heavy Rare-Earth Chromite RECrO<sub>3</sub> (RE = Er, Tm, Yb,) Tj ETQq0 0 0 rgBT /Overlock 10 20

59	A validated LC–MS/MS method for the simultaneous determination of BMS-791325, a hepatitis C virus NS5B RNA polymerase inhibitor, and its metabolite in plasma. Journal of Chromatography B: Analytical Technologies in the Biomedical and Life Sciences, 2014, 973, 1-8.	2.3	19
60	Mineralizer effect on facet-controllable hydrothermal crystallization of perovskite structure YbFeO <sub>3</sub> crystals. CrystEngComm, 2018, 20, 470-476.	2.6	19
61	Size-dependent optical and thermochromic properties of Sm <sub>3</sub> Fe <sub>5</sub> O <sub>12</sub> . RSC Advances, 2017, 7, 37765-37770.	3.6	17
62	Improved ruggedness of an ionâ€pairing liquid chromatography/tandem mass spectrometry assay for the quantitative analysis of the triphosphate metabolite of a nucleoside reverse transcriptase inhibitor in peripheral blood mononuclear cells. Rapid Communications in Mass Spectrometry, 2013, 27, 481-488.	1.5	16
63	A rugged and accurate liquid chromatography–tandem mass spectrometry method for the determination of asunaprevir, an NS3 protease inhibitor, in plasma. Journal of Chromatography B: Analytical Technologies in the Biomedical and Life Sciences, 2013, 921-922, 81-86.	2.3	16
64	The effect of NH <sub>4</sub> <sup>+</sup> on shape modulation of La <sub>1â^'x</sub> Sr <sub>x</sub> MnO <sub>3</sub> crystals in a hydrothermal environment. CrystEngComm, 2014, 16, 9842-9846.	2.6	16
65	Hydrothermal synthesis, morphology, structure, and magnetic properties of perovskite structure LaCr <sub>1â^x</sub> Mn <sub>x</sub> O <sub>3</sub> ( <i>x</i> = 0.1, 0.2, and 0.3). CrystEngComm, 2018, 20, 3034-3042.	2.6	16
66	<i>In situ</i> exsolution of Ag from AgBiS <sub>2</sub> nanocrystal anode boosting high-performance potassium-ion batteries. Journal of Materials Chemistry A, 2020, 8, 15058-15065.	10.3	16
67	Shape tuneable synthesis of perovskite structured rare-earth chromites RECrO <sub>3</sub> via a mild hydrothermal method. CrystEngComm, 2017, 19, 6436-6442.	2.6	15
68	Design Principles for 3d Electron Transfer in a Ga-Based Garnet To Enable High-Performance Reversible Thermochromic Material Color Maps. Chemistry of Materials, 2019, 31, 1048-1056.	6.7	15
69	Green catalyst: magnetic La <sub>0.7</sub> Sr <sub>0.3</sub> MnO <sub>3</sub> hollow microspheres. New Journal of Chemistry, 2015, 39, 2413-2416.	2.8	14
70	Architecture of Biomimetic Water Oxidation Catalyst with Mn <sub>4</sub> CaO <sub>5</sub> Clusterlike Structure Unit. ACS Applied Materials & Interfaces, 2018, 10, 37948-37954.	8.0	14
70 71	Architecture of Biomimetic Water Oxidation Catalyst with Mn <sub>4</sub> CaO <sub>5</sub> Clusterlike Structure Unit. ACS Applied Materials & amp; Interfaces, 2018, 10, 37948-37954. Graphene Oxide Induced High Crystallinity of SAPOâ€11 Molecular Sieves for Improved Alkane Isomerization Performance. ChemNanoMat, 2019, 5, 1225-1232.	<b>8.0</b> 2.8	14 14

#	Article	IF	CITATIONS
73	Manipulation of Exciton Dynamics in Single-Layer WSe <sub>2</sub> Using a Toroidal Dielectric Metasurface. Nano Letters, 2021, 21, 9930-9938.	9.1	14
74	Automation in new frontiers of bioanalysis: a key for quality and efficiency. Bioanalysis, 2012, 4, 2759-2762.	1.5	13
75	A simple, effective approach for rapid development of high-throughput and reliable LC–MS/MS bioanalytical assays. Bioanalysis, 2016, 8, 1809-1822.	1.5	13
76	Hydrothermal synthesis and magnetic behaviour of beta-Li3VF6 and Na3VF6. New Journal of Chemistry, 2015, 39, 5080-5083.	2.8	12
77	Hydrothermal shape controllable synthesis of La <sub>0.5</sub> Sr <sub>0.5</sub> MnO <sub>3</sub> crystals and facet effect on electron transfer of oxygen reduction. Inorganic Chemistry Frontiers, 2018, 5, 732-738.	6.0	12
78	Size tunable Ga–Ge nanowires for Li-ion battery prepared by in situ alloying in ionic liquid electrodeposition. Applied Surface Science, 2020, 508, 144852.	6.1	12
79	Use of a carboxylesterase inhibitor of phenylmethanesulfonyl fluoride to stabilize epothilone D in rat plasma for a validated UHPLC–MS/MS assay. Journal of Chromatography B: Analytical Technologies in the Biomedical and Life Sciences, 2014, 969, 60-68.	2.3	11
80	Shape Control of Ternary Sulfide Nanocrystals. Crystal Growth and Design, 2018, 18, 864-871.	3.0	11
81	Hydrothermal Synthesized Co-Ni3S2 Ultrathin Nanosheets for Efficient and Enhanced Overall Water Splitting. Chemical Research in Chinese Universities, 2019, 35, 179-185.	2.6	11
82	Reversible thermochromic property of Cr, Mn, Fe, Co-doped Ca <sub>14</sub> Zn <sub>6</sub> Ga <sub>10</sub> O <sub>35</sub> . Journal of Materials Chemistry C, 2020, 8, 9615-9624.	5.5	11
83	In Situ Spectroscopic Ellipsometry for Thermochromic CsPbI <sub>3</sub> Phase Evolution Portfolio. Journal of Physical Chemistry C, 2020, 124, 8008-8014.	3.1	11
84	Validation and application of hybridization liquid chromatography-tandem mass spectrometry methods for quantitative bioanalysis of antisense oligonucleotides. Bioanalysis, 2022, 14, 589-601.	1.5	11
85	Luminescent properties of LaKNaTaO5 and rare-earth-doped LaKNaTaO5 synthesized by an improved hydroxide melt method. Journal of Luminescence, 2013, 135, 196-200.	3.1	10
86	Photoluminescence properties of BaSiF <sub>6</sub> :Eu <sup>3+</sup> ,Eu <sup>3+</sup> /K <sup>+</sup> and Eu <sup>3+</sup> /Tb <sup>3+</sup> co-doped phosphors. New Journal of Chemistry, 2015, 39, 9071-9074.	2.8	10
87	Effect of Ca dopant on magnetic and magnetodielectric properties of Y3Fe5O12. Journal of Alloys and Compounds, 2021, 861, 157996.	5.5	10
88	Feasibility assessment of a novel selective peptide derivatization strategy for sensitivity enhancement for the liquid chromatography/tandem mass spectrometry bioanalysis of protein therapeutics in serum. Rapid Communications in Mass Spectrometry, 2014, 28, 705-712.	1.5	9
89	UV–vis absorption shift of mixed valance state tungstate oxide: Ca0.72La0.28WO4. Materials Letters, 2015, 143, 212-214.	2.6	9
90	Investigation of the "true―extraction recovery of analytes from multiple types of tissues and its impact on tissue bioanalysis using two model compounds. Analytica Chimica Acta, 2016, 945, 57-66.	5.4	9

#	Article	IF	CITATIONS
91	Phaseâ€Controlled Synthesis of Highâ€Biâ€Ratio Ternary Sulfide Nanocrystals of Cu <sub>1.57</sub> Bi <sub>4.57</sub> S <sub>8</sub> and Cu <sub>2.93</sub> Bi <sub>4.89</sub> S <sub>9</sub> . ChemPlusChem, 2018, 83, 812-818.	2.8	9
92	A convenient strategy to overcome interference in LC-MS/MS analysis: Application in a microdose absolute bioavailability study. Journal of Pharmaceutical and Biomedical Analysis, 2019, 165, 198-206.	2.8	9
93	Application of in-sample calibration curve methodology for regulated bioanalysis: Critical considerations in method development, validation and sample analysis. Journal of Pharmaceutical and Biomedical Analysis, 2020, 177, 112844.	2.8	9
94	The direct synthesis of Au nanocrystals in microdroplets using the spray-assisted method. New Journal of Chemistry, 2016, 40, 7294-7298.	2.8	8
95	Electric-field-induced assembly of Ag nanoparticles on a CuO nanowire using ambient electrospray ionization. New Journal of Chemistry, 2017, 41, 2878-2882.	2.8	8
96	B-site ordering, magnetic and dielectric properties of hydrothermally synthesized Lu2NiMnO6. Journal of Alloys and Compounds, 2018, 744, 395-403.	5.5	8
97	Hydrothermal growth of facet-tunable fluoride perovskite crystals KMF3 (M = Mg, Mn, Co, Ni and Zn). CrystEngComm, 2020, 22, 6216-6227.	2.6	8
98	Shape Controllable Synthesis of Bi-Based Perovskite Superconductor Microcrystals via a Mild Hydrothermal Method. Crystal Growth and Design, 2020, 20, 2123-2128.	3.0	8
99	In-Situ thermochromic mechanism of Spin-Coated VO2 film. Applied Surface Science, 2021, 564, 150441.	6.1	8
100	A UHPLC–MS/MS bioanalytical assay for the determination of BMS-911543, a JAK2 inhibitor, in human plasma. Journal of Chromatography B: Analytical Technologies in the Biomedical and Life Sciences, 2015, 991, 85-91.	2.3	7
101	Discovery, identification and mitigation of isobaric sulfate metabolite interference to a phosphate prodrug in LC–MS/MS bioanalysis: Critical role of method development in ensuring assay quality. Journal of Pharmaceutical and Biomedical Analysis, 2018, 155, 141-147.	2.8	7
102	Hydrothermal synthesis and magnetic properties of SmCr0.5M0.5O3(M=Fe and Mn) micro-plates. Chemical Research in Chinese Universities, 2018, 34, 1-7.	2.6	7
103	Optimization of oxygen evolution dynamics on RuO <sub>2</sub> <i>via</i> controlling of spontaneous dissociation equilibrium. Materials Chemistry Frontiers, 2019, 3, 1779-1785.	5.9	7
104	Oxygen vacancies enhancing acetone-sensing performance. Materials Today Chemistry, 2020, 18, 100372.	3.5	7
105	Fit-for-purpose protein biomarker assay validation strategies using hybrid immunocapture-liquid chromatography-tandem-mass spectrometry platform: Quantitative analysis of total soluble cluster of differentiation 73. Analytica Chimica Acta, 2020, 1126, 144-153.	5.4	7
106	Challenges and recommendations in developing LC–MS/MS bioanalytical assays of labile glucuronides and parent compounds in the presence of glucuronide metabolites. Bioanalysis, 2020, 12, 615-624.	1.5	7
107	Antisense Oligonucleotide In Vitro Protein Binding Determination in Plasma, Brain, and Cerebral Spinal Fluid Using Hybridization LC-MS/MS. Drug Metabolism and Disposition, 2022, 50, 268-276.	3.3	7
108	Luminescence Enhancement of Lu <sub>3</sub> TaO <sub>7</sub> :Eu <sup>3+</sup> @Lu <sub>3</sub> TaO <sub>7</sub> Redâ€Emitting Nanophosphors. European Journal of Inorganic Chemistry, 2015, 2015, 690-695.	2.0	6

#	Article	IF	CITATIONS
109	Fabrication and In vitro Bioactivity of Robust Hydroxyapatite Coating on Porous Titanium Implant. Chemical Research in Chinese Universities, 2019, 35, 686-692.	2.6	6
110	Soft-Chemical Method for Synthesizing Intermetallic Antimonide Nanocrystals from Ternary Chalcogenide. Langmuir, 2019, 35, 15131-15136.	3.5	6
111	Moisture-stimulated reversible thermochromic CsPbI3-xBrx films: In-situ spectroscopic-resolved structure and optical properties. Applied Surface Science, 2022, 573, 151484.	6.1	6
112	Surface reconstruction: An effective method for the growth of mismatched materials. Applied Surface Science, 2016, 360, 547-552.	6.1	5
113	Nd3â^'xAExFe5O12: Hydrothermal synthesis, structure and magnetic properties. Chemical Research in Chinese Universities, 2017, 33, 869-875.	2.6	5
114	Morphology, Structure Evolution and Siteâ€Selective Occupancy of Eu 3+ in Ca 10 (PO 4 ) 6 (OH) 2 Nanorods Synthesized via Subcritical Hydrothermal Method. ChemistrySelect, 2018, 3, 7749-7756.	1.5	5
115	Activity adaptability of a DhHP-6 peroxidase-mimic in wide pH and temperature ranges and solvent media. Catalysis Science and Technology, 2020, 10, 1848-1857.	4.1	5
116	Tuneable colour-emitting Ce3+, Eu3+/K+ and Ce3+/Tb3+ doped BaSiF6 phosphors via charge compensation and energy transfer. Journal of Luminescence, 2018, 198, 203-207.	3.1	4
117	Thermal stable blue pigment with tunable color of DyIn1-xMnxO3 (0≤≤0.1). Dyes and Pigments, 2018, 156, 192-198.	3.7	4
118	Fabrication of ultralong perovskite structure nanotubes. RSC Advances, 2018, 8, 367-373.	3.6	4
119	Overcoming the stability, solubility and extraction challenges in reversed-phase UHPLC–MS/MS bioanalysis of a phosphate drug and its prodrug in blood lysate. Journal of Pharmaceutical and Biomedical Analysis, 2018, 157, 36-43.	2.8	4
120	<i>In situ</i> Ga-alloying in germanium nano-twists by the inhibition of fractal growth with fast Li <sup>+</sup> -mobility. Chemical Communications, 2019, 55, 10412-10415.	4.1	4
121	Dried blood spot analysis without dilution: Application to the LC–MS/MS determination of BMS-986001 in rat dried blood spot. Journal of Chromatography B: Analytical Technologies in the Biomedical and Life Sciences, 2015, 1002, 201-209.	2.3	3
122	Molecular beam epitaxial growth of oriented and uniform Ge2Sb2Te5 nanoparticles with compact dimensions. Journal of Nanoparticle Research, 2017, 19, 1.	1.9	3
123	Tuning the interfacial and energetic interactions between a photoexcited conjugated polymer and open-shell small molecules. Soft Matter, 2019, 15, 1413-1422.	2.7	3
124	Quantitative Bioanalysis of Proteins by Mass Spectrometry. Materials and Methods, 0, 5, .	0.0	3
125	Revealing charge carrier dynamics and transport in Te-doped GaAsSb and GaAsSbN nanowires by correlating ultrafast terahertz spectroscopy and optoelectronic characterization. Nanotechnology, 2022, 33, 425702.	2.6	3
126	Infrared Absorption Enhancement by Charge Transfer in Ga-GaSb Metal-Semiconductor Nanohybrids. Langmuir, 2016, 32, 4189-4193.	3.5	2

#	Article	IF	CITATIONS
127	A bridging immunogenicity assay for anti-cabiralizumab antibodies: overcoming the low assay cut point and drug tolerance challenges. Bioanalysis, 2021, 13, 395-407.	1.5	2
128	Bioanalysis Young Investigator: Announcing our finalists!. Bioanalysis, 2013, 5, 1963-1964.	1.5	1
129	Design and synthesis of metal hydroxide three-dimensional inorganic cationic frameworks. Dalton Transactions, 2018, 47, 3339-3345.	3.3	1
130	Tensile and biodegradable properties of Mg-6.0Zn-1.0Nd-0.5Zr alloy. Inorganic Chemistry Communication, 2021, 123, 108337.	3.9	1
131	Open-air solvothermal synthesis and photoresponse of plate-shaped Cu3ZnInSnSe6 nanocrystals. Journal of Nanoparticle Research, 2021, 23, 1.	1.9	1
132	Pourbaix-Guided Mineralization and Site-Selective Photoluminescence Properties of Rare Earth Substituted B-Type Carbonated Hydroxyapatite Nanocrystals. Molecules, 2021, 26, 540.	3.8	1
133	Improved energy conversion efficiency of ZnO/polythiophene solar cell in Ga-doped ZnO nanorod array photoanode. Chemical Research in Chinese Universities, 2016, 32, 979-984.	2.6	Ο
134	Hydrothermal Growth of Centimeter-Scale CuO Plates: Planar Chromium(III) Oligomer as a Facet-Directing Agent. Inorganic Chemistry, 2018, 57, 2957-2960.	4.0	0
135	Manipulation of Exciton Dynamics and Annihilation in Single-Layer WSe2 using a Toroidal Dielectric Metasurface. , 2021, , .		0